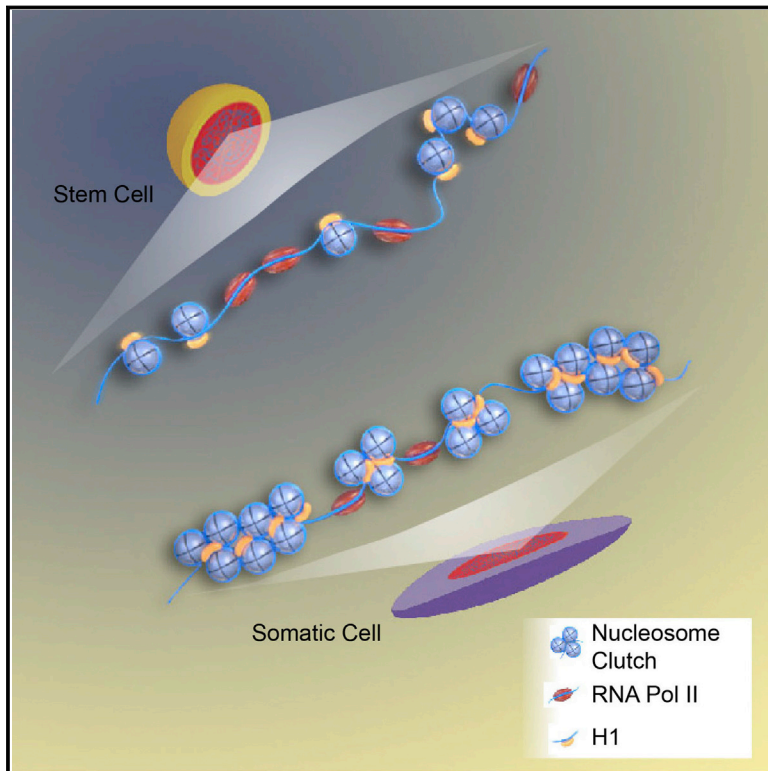


Chromatin Fibers Are Formed by Heterogeneous Groups of Nucleosomes In Vivo

Graphical Abstract



Authors

Maria Aurelia Ricci, Carlo Manzo, ..., Melike Lakadamyali, Maria Pia Cosma

Correspondence

melike.lakadamyali@icfo.es (M.L.),
pia.cosma@crg.es (M.P.C.)

In Brief

Nucleosomes associate in discrete clutches along the chromatin fiber and clutch size correlates with cell pluripotency.

Highlights

- Nucleosomes are arranged in heterogeneous clutches along the chromatin fiber
- The median number of nucleosomes per clutch in a given nucleus is cell-specific
- Larger and denser clutches form the “closed” heterochromatin
- Nucleosome-depleted regions separate nucleosome clutches



Chromatin Fibers Are Formed by Heterogeneous Groups of Nucleosomes In Vivo

Maria Aurelia Ricci,^{1,2,5} Carlo Manzo,^{3,5} María Filomena García-Parajo,^{3,4} Melike Lakadamyali,^{3,6,*} and Maria Pia Cosma^{1,2,4,6,*}

¹Centre for Genomic Regulation (CRG), Dr Aiguader 88, 08003 Barcelona, Spain

²Universitat Pompeu Fabra (UPF), Dr Aiguader 88, 08003 Barcelona, Spain

³ICFO, Institut de Ciències Fotòniques, Mediterranean Technology Park, 08860 Castelldefels, Barcelona, Spain

⁴Institució Catalana de Recerca i Estudis Avançats (ICREA), 08010 Barcelona, Spain

⁵Co-first author

⁶Co-senior author

*Correspondence: melike.lakadamyali@icfo.es (M.L.), pia.cosma@crg.es (M.P.C.)

<http://dx.doi.org/10.1016/j.cell.2015.01.054>

SUMMARY

Nucleosomes help structure chromosomes by compacting DNA into fibers. To gain insight into how nucleosomes are arranged in vivo, we combined quantitative super-resolution nanoscopy with computer simulations to visualize and count nucleosomes along the chromatin fiber in single nuclei. Nucleosomes assembled in heterogeneous groups of varying sizes, here termed “clutches,” and these were interspersed with nucleosome-depleted regions. The median number of nucleosomes inside clutches and their compaction defined as nucleosome density were cell-type-specific. Ground-state pluripotent stem cells had, on average, less dense clutches containing fewer nucleosomes and clutch size strongly correlated with the pluripotency potential of induced pluripotent stem cells. RNA polymerase II preferentially associated with the smallest clutches while linker histone H1 and heterochromatin were enriched in the largest ones. Our results reveal how the chromatin fiber is formed at nanoscale level and link chromatin fiber architecture to stem cell state.

INTRODUCTION

Eukaryotic nucleosomes are a repeating unit of the chromatin, formed by 146 base pairs (bp) of DNA wrapped around octamers of the four core histone proteins (H2A, H2B, H3, and H4) (Luger et al., 1997). The histone H1 binds DNA entry/exit points of nucleosomes and to linker DNA between nucleosomes to compact the chromatin (Woodcock et al., 2006). According to the “textbook picture,” chromatin compaction follows a hierarchical model where nucleosomes form a “beads-on-string” fiber of 10 nm in diameter, which folds into higher ordered fibers of 30 nm, which in turn compact progressively into larger fibers of 100–200 nm (Finch and Klug, 1976; Song et al., 2014; Widom, 1992).

The existence of this hierarchical organization inside intact eukaryotic nuclei in vivo has recently been debated after cryo-electron microscopy, small-angle X-ray scattering (SAXS), and electron spectroscopic imaging experiments failed to detect the 30-nm fiber (Efroni et al., 2008; Fussner et al., 2012; Joti et al., 2012; Nishino et al., 2012). These studies led to the overall conclusion that the eukaryotic nuclei are mainly composed of 10 nm fibers even though the core histone proteins could not be identified unequivocally using these methods due to their lack of molecular specificity. In addition, genome-wide analyses have revealed that nucleosomes are depleted at promoter and terminator regions and at many enhancers (Struhl and Segal, 2013). Since the 30-nm fiber arrangement imposes specific constraints on nucleosome occupancy and positioning (Fussner et al., 2011a), genome-wide analyses along with the latest imaging results argue against a hierarchical organization of nucleosomes along the chromatin fiber. However, due to the limitations of previous approaches, which either lack molecular specificity or are based on population studies, histones have not been specifically visualized in intact nuclei and thus the organization of nucleosomes along the chromatin fiber has not been resolved so far.

Here, we used super-resolution nanoscopy (stochastic optical reconstruction microscopy [STORM]) (Rust et al., 2006) to visualize the structure of the chromatin fiber of a large variety of different cells at single cell level with a resolution of ~20 nm by imaging the core histone protein H2B. Super-resolution has previously been used to visualize chromatin in interphase (Bohn et al., 2010; Wombacher et al., 2010) and in dividing nuclei (Matsuda et al., 2010). Up to date, however, super-resolution studies of chromatin have not addressed questions regarding the organization of single or groups of nucleosomes, the overall nucleosome occupancy level of DNA and whether these parameters are consistent with the 30-nm fiber. Moreover, how the chromatin organization changes at the nanoscale level as a function of cell state such as pluripotent or differentiated state, while of fundamental significance for DNA accessibility and gene expression, has not yet been addressed. Overall, a quantitative approach that can estimate the number of nucleosomes within the chromatin fiber and thus identify nucleosome spatial arrangement has been lacking.

Our observations indicate that nucleosomes are grouped in discrete domains along the chromatin fiber, which we termed “nucleosome clutches” in analogy with “egg clutches.” Clutches are interspersed with nucleosome-depleted regions and the number of nucleosomes per clutch is very heterogeneous in a given nucleus arguing against the existence of a well-organized and ordered fiber. These observations were validated by computer simulations, which were also used to estimate the nucleosome occupancy of the chromatin fiber. Two-color STORM showed increased levels of H1 in larger and denser clutches containing more nucleosomes, which formed the “closed” heterochromatin. On the other hand, “open” chromatin was formed by smaller and less dense clutches which associated with RNA Polymerase II. Strikingly, despite the heterogeneity in clutch size in a given nucleus, on average differentiated cells contained larger and denser clutches compared to stem cells. These results reveal the nanoscale architecture of the chromatin fiber by showing how nucleosomes are arrayed in intact interphase nuclei.

RESULTS

Nucleosomes in Interphase Nuclei of Human Somatic Cells Are Organized in Discrete Nanodomains

To reveal the organization of chromatin at nanoscale resolution, we recorded STORM images of the core histone protein H2B in interphase human fibroblast nuclei (hFb) since H2B is one of the histones with fewer tail modifications and functional variants with known function (Kamakaka and Biggins, 2005). STORM images revealed a striking organization of H2B inside the nucleus (Figure 1A, left), which was not evident with conventional fluorescence microscopy (Figure S1A). H2B appeared clustered in discrete and spatially separated nanodomains (Figure 1A, left zooms). The H2B nanodomain density (number of nanodomains per unit area) was ~25% higher in the nuclear periphery, where the heterochromatin is thought to be located, compared to the nuclear interior. Since H2B is a core histone of the nucleosome octamer, its localization should reflect the arrangement of nucleosomes within the chromatin fiber. Accordingly, another core histone protein of the nucleosome octamer, H3, was similarly clustered in discrete nanodomains (Figure S1B). Furthermore, as expected, ~85% of H3 co-localized with H2B (Figure S1C).

To rule out the possibility that the observed clustered distribution of H2B was due to sample preparation or labeling methods used, we performed a series of control experiments. First, the clustered distribution of H2B was independent of the fixation and permeabilization protocols used (Figures S1D and S1E). Second, STORM images contained discrete nanodomains when H2B was indirectly labeled using an antibody against SNAP tag in cells stably expressing H2B-SNAP (Figure S1F). Third, we ruled out potential artifacts in H2B STORM images associated with the large size of the antibody by comparing to nanobody labeling (Figures S1G–S1N). Fourth, labeling efficiency defects were also ruled out by computer simulations of nucleosome arrangements (see further details in [Extended Experimental Procedures](#) and [DNA Fiber Is Not Fully Occupied with Nucleosomes](#) section). Finally, to confirm the existence of H2B nanodomains in living cells we imaged H2B-mEos2 or

H2B-PA-mCherry expressing hFbs. In both cases super-resolution imaging revealed discrete and spatially separated nanodomains as in the case of fixed cells (Figures 1B and S1O).

We next analyzed the nucleosome organization in cells undergoing massive epigenome modifications and chromatin rearrangements. For this, hFbs were treated with Trichostatin A (TSA) (TSA-hFb), a potent inhibitor of histone deacetylase enzyme, which leads to genome-wide decondensation of chromatin through accumulation of acetylation groups on histone tails (Tóth et al., 2004). As expected, there was a large increase in H3 acetylation after TSA treatment (Figure S1P). TSA treatment also resulted in visually evident changes in the nuclear distribution of H2B nanodomains (Figure 1A, right), which appeared dimmer and hence contained less localizations. Furthermore, the nanodomains were also more dispersed within the nucleus (Figure 1A, right zooms). The H2B nanodomain density was enhanced by ~10% in the nuclear periphery of TSA-hFbs compared to the nuclear interior, although it was less dense than the nuclear periphery of untreated hFbs. Finally, the distribution of acetylated H3 was also highly dispersed in the nuclei, mirroring the spatial re-distribution observed for the H2B nanodomains after TSA treatment (Figure S1P). These changes overall indicate that nucleosomes undergo spatial rearrangement in hFb nuclei upon chromatin decondensation.

To gain quantitative insight into the H2B nanodomains, we next developed a cluster identification algorithm to group the localizations in STORM images into nanodomains ([Extended Experimental Procedures](#); Figures 1C and S1Q). Quantitative analysis revealed that the distributions of the number of localizations per nanodomain, nanodomain areas, and nanodomain nearest neighbor distances (nnds) were shifted to lower values in TSA-hFbs compared to hFbs (Figure 1D), and hence nucleosomes showed statistically significant spatial re-organization after TSA treatment and chromatin decondensation.

In control experiments, nanodomain areas of hFbs were similar when H2B was labeled with an antibody (Mean Area \pm SEM = 830 ± 70 nm², n = 11 cells), with GFP-nanobody in hFbs transfected with H2B-GFP (Mean Area \pm SEM = 660 ± 70 nm², n = 7 cells, p = 0.1760) and in living or fixed hFbs expressing H2B-mEos2 or H2B-PA-mCherry (Mean Area \pm SEM = 660 ± 30 nm² in living cells, n = 12 cells, p = 0.068 and 610 ± 40 nm² in fixed cells, n = 5 cells, p = 0.1088, Figure S1R), indicating that the large size of the antibody or fixation did not significantly affect the spatial resolution of H2B STORM images or the organization of nanodomains. The number of localizations per nanodomain was lower when using fluorescent proteins compared to organic fluorophores as expected (Figure S1R), since mEos2 and PA-mCherry are known to undergo less blinking and photoactivate with only moderate efficiency (Durisic et al., 2014) compared to AlexaFluor647.

Wild-Type Mouse Embryonic Stem Cells Cultured under Different Media Conditions and Mutants Have Distinct Nucleosome Organization in Interphase

To assess the nucleosome organization of pluripotent cells, we next imaged H2B in mouse embryonic stem cells (mESCs). mESCs were cultured under two different media conditions: (1) with serum and the cytokine leukemia inhibitory factor (sLif),

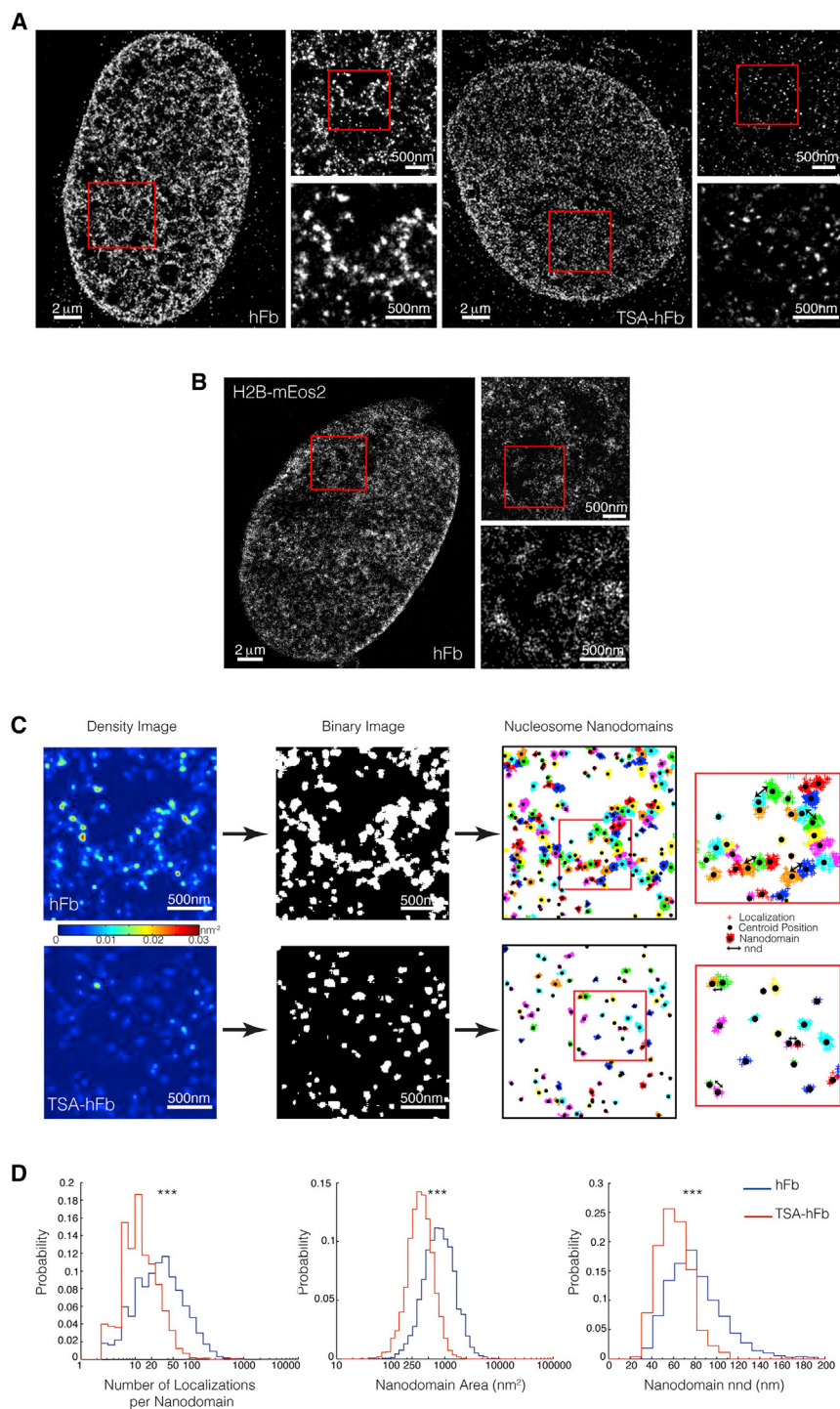


Figure 1. Nucleosomes Are Arranged in Discrete Nanodomains in Interphase Nuclei of Human Somatic Cells

(A) Representative STORM images of H2B in human fibroblast nucleus (hFb, left) ($n = 11$ cells) and Trichostatin A (TSA)-treated human fibroblast nucleus (TSA-hFb, right) ($n = 11$ cells). Progressively higher zooms of the regions inside the red squares are shown next to each nucleus.

(B) Live cell super-resolution images of hFbs expressing H2B-mEos2. Progressively higher zooms of the regions inside the red squares are shown next to each nucleus.

(C) Density images showing regions of high (red) and low (blue) H2B density (number of H2B localizations per unit area) in hFb (upper) and TSA-hFb (lower) according to the color scale bar. After thresholding, the density images are converted into binary images in which regions containing H2B localizations appear white. Every white region is analyzed using a cluster identification algorithm that groups the individual localizations based on their proximity into nanodomains. Shown are example nanodomains in hFb (upper) and TSA-hFb (lower) for which localizations (crosses) having the same color belong to the same nanodomain. The centroid position of each nanodomain is shown as a black dot. The nearest neighbor distances (nnds) between nanodomains inside the white regions are calculated (double head black arrows), along with the number of localizations per nanodomain and the nanodomain area.

(D) Representative distributions of the number of H2B localizations per nanodomain, nanodomain area, and nnds between nanodomains in hFb (blue) and TSA-hFb (red) for the cells shown in (A). Statistical significance between the different distributions is shown as *** ($p < 10^{-3}$).

See also [Figure S1](#).

gram of their transcriptional profile and a more homogenous expression of pluripotency factors ([Marks et al., 2012](#); [Wray et al., 2010](#)).

As expected, mESCs cultured in sLif expressed varying levels of the pluripotency marker Nanog ([Figure S2A](#)). Low Nanog expressing cells ([Figure S2A](#), upper) had bright nanodomains in STORM images (i.e., containing a large number of localizations) ([Figure 2A](#), type 1, yellow arrowheads). On the other hand, high Nanog expressing mESCs cultured in sLif ([Figure S2A](#), lower) mostly had dim

and (2) with inhibitors of two kinases (Mek and Gsk3) known as “2i” and Lif (2iLif). mESCs cultured in sLif have heterogeneous morphology, exhibit heterogeneous expression of pluripotency factors ([Cahan and Daley, 2013](#)), and display appreciable expression of ectoderm and mesoderm genes ([Marks et al., 2012](#)). On the other hand, 2iLif maintains mESCs in a ground-state ([Ying et al., 2008](#)), characterized by no predetermined pro-

nanodomains ([Figure 2B](#), type 2, cyan arrowheads). In addition, the nanodomains appeared more dispersed inside the nucleus. Nanodomains of mESCs cultured in 2iLif and of mESCs^{Tcf3^{-/-}} were mostly dim ([Figures 2C](#), [2D](#), and [2G](#)). Similar to 2iLif, the deletion of Tcf3 (mESCs^{Tcf3^{-/-}}), a key effector of the Wnt/ β -catenin pathway, was also previously shown to maintain the ground-state of pluripotency ([Cole et al., 2008](#); [Tam et al.,](#)

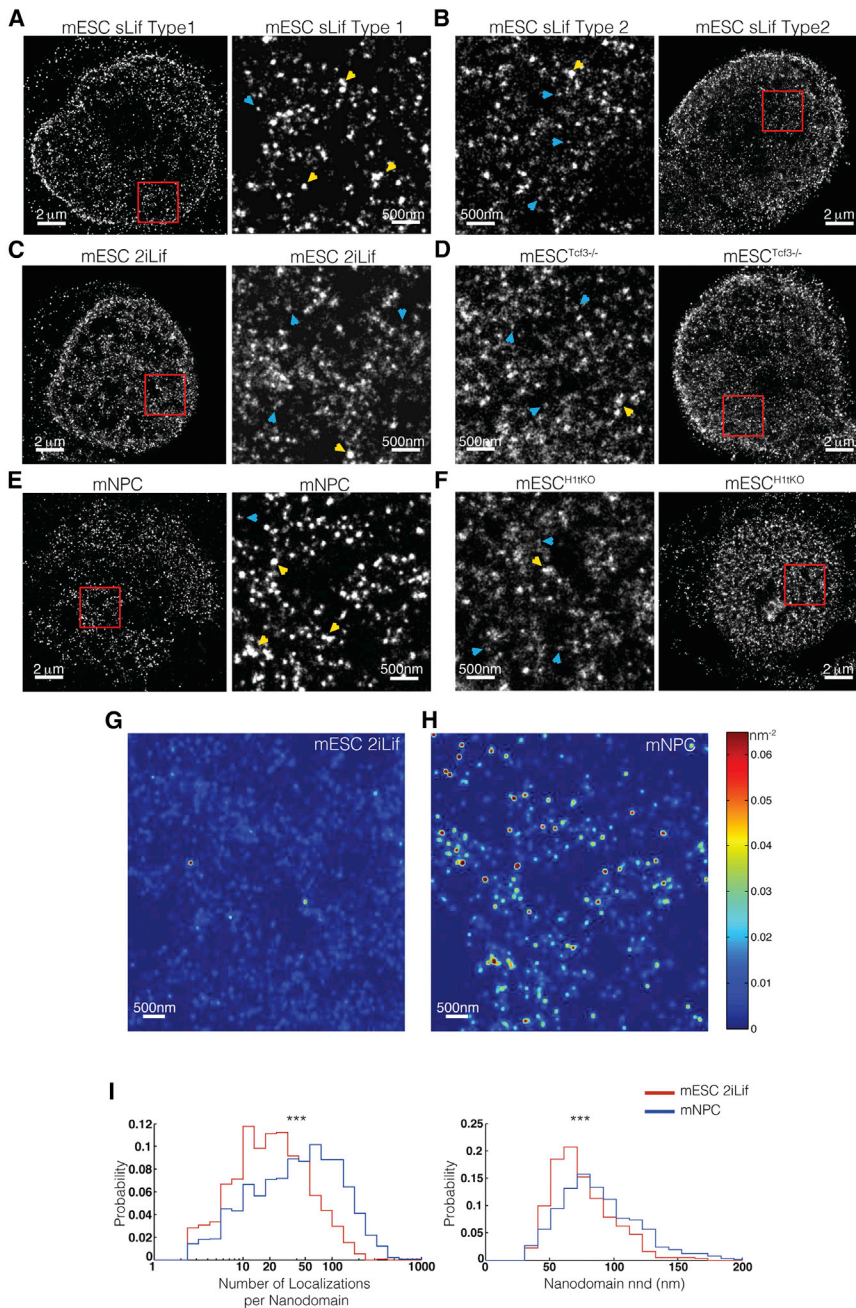


Figure 2. Nucleosomes Are Arranged in Discrete Nanodomains in Interphase Nuclei of Mouse Embryonic Stem Cells

(A–F) Representative STORM images of H2B in (A) type 1 mouse embryonic stem cells (mESCs) cultured in serum plus Lif (sLif) ($n = 8$ cells), (B) type 2 mESCs cultured in sLif ($n = 6$ cells), (C) mESCs cultured in 2iLif ($n = 15$ cells), (D) mutant mESCs lacking Tcf3 (mESC^{Tcf3-/-}) ($n = 10$ cells), (E) neuronal precursor cells (mNPC) obtained after differentiation of mESCs ($n = 9$ cells), and (F) mutant mESCs that are triple H1 knockout (mESC^{H1^{tko}}) ($n = 15$ cells). Next to each cell type, higher zooms of the regions inside the red squares are shown. Yellow arrowheads point to bright nanodomains comprising a large number of localizations whereas cyan arrowheads point to dimmer nanodomains comprising a small number of localizations.

(G and H) Density image showing the differences in nanodomain organization of mESCs cultured in 2iLif (G) and mNPCs (H). Regions of high (red) and low (blue) H2B density are shown according to the color scale bar.

(I) Representative distributions of the number of H2B localizations per nanodomain and nanodomain nnds in mESCs cultured in 2iLif medium (red) and mNPCs (blue) for the cells shown in (C) and (E). Statistical significance is shown as *** ($p < 10^{-3}$). See also [Figure S2](#).

Taken together, these results indicate that the chromatin in ground-state mESCs is characterized by dimmer H2B nanodomains, which are more dispersed inside the nuclear space and by increased acetylation level.

The linker histone H1 is thought to play an important role in chromatin organization and higher order compaction ([Clau-sell et al., 2009](#); [Woodcock et al., 2006](#)). mESCs carrying a deletion of three H1 isoforms (mESC^{H1^{tko}}), which were shown to have reduced chromatin compaction ([Fan et al., 2005](#)) contained a large amount of dim nanodomains ([Figure 2F](#)) having a similar organization to those observed in mESCs cultured in 2iLif and in mESCs^{Tcf3-/-}.

Quantitative analysis also confirmed that the number of localizations per nanodomain and nanodomain nnds were lower in ground-state mESCs with respect to somatic mNPCs ([Figures 2I and 3](#), below).

Nanodomains Contain a Discrete Number of Nucleosomes and the Nucleosome Number Correlates with Pluripotency

Given the identical labeling and imaging conditions used for each cell type ([Extended Experimental Procedures](#); [Table S1](#)), the number of nucleosomes should scale with the number of

2008; [Yi et al., 2008](#)). When mESCs were differentiated into neural precursor cells (mNPCs) the H2B nanodomains became brighter, resembling those observed in hFbs ([Figures 2E and 2H](#)).

ESCs^{Tcf3-/-} were shown to contain large epigenome modifications ([Lluis et al., 2011](#)). Accordingly, there was increased level of acetylation in these cells ([Figure S2B](#)) with respect to type 1 mESCs cultured in sLif ([Figure S2C](#)). mESCs cultured in 2iLif ([Figure S2D](#)) as well as type 2 mESCs cultured in sLif ([Figure S2E](#)) also contained higher levels of H3 acetylation, while mNPCs showed a lower level of H3 acetylation ([Figure S2F](#)).

localizations (Dani et al., 2010). Nanodomains in any given nucleus contained a large distribution of localizations spanning two orders of magnitude (~ 3 to 300) (Figures 1D and 2I), indicating that they comprised heterogeneous groups with varying numbers of nucleosomes. We will refer to these heterogeneous nucleosome groups as “nucleosome clutches” in analogy to “egg clutches” and we will use the term “clutch size” interchangeably with the number of nucleosomes per clutch. Despite this heterogeneity, the median number of localizations per clutch in individual cells correlated strongly with cell type and showed statistically significant differences between hFbs and TSA-hFbs and among the different mESCs (Figures 3A and 3B). Control experiments showed that the median number of localizations per clutch in hFbs was similar when H3 was labeled ($N_{\text{localizations}} = 24 \pm 2$) instead of H2B ($N_{\text{localizations}} = 24 \pm 4$) and under different fixation and permeabilization conditions ($N_{\text{localizations}} = 24 \pm 4$ for ethanol/methanol fixation, $N_{\text{localizations}} = 26 \pm 3$ for PFA fixation), excluding potential sample labeling artifacts.

Overall, the differences in the median numbers of localizations indicate that nucleosomes assemble into clutches of larger size in hFbs compared to TSA-hFbs (Figure 3A). Similarly, nucleosomes formed larger clutches in differentiated mNPCs and mESCs cultured in sLif compared to mESCs cultured in 2iLif, mESC^{Tcf3^{-/-}} and mESC^{H1tKO} (Figure 3B).

In order to relate the median number of localizations to the median number of nucleosomes in different cell types, we further generated a calibration curve by imaging in vitro-labeled mononucleosomes and polynucleosome arrays containing 12- or 24-nucleosomes (Grigoryev et al., 2009) (Extended Experimental Procedures; Figures S3A–S3C). Mononucleosomes had a median number of ten localizations, indicating a high detection efficiency of single nucleosomes using STORM. We also labeled and imaged the 12- and 24-polynucleosome arrays in the presence of nuclear extract to better emulate the crowding of the nuclear environment (Extended Experimental Procedures). A similar median number of localizations was obtained in the presence of the extract (Figures 3C, S3B, and S3D) reassuring that labeling efficiency does not significantly differ under both conditions. The calibration curve was also validated by imaging a plasmid with a length allowing the assembly of ~ 20 nucleosomes. The median number of localizations obtained corresponded to 19.5 ± 2 nucleosomes after interpolation, confirming that the calibration curve was indeed accurate (Figure 3C). We also estimated that on average 1.6 antibodies (1/0.6) were present on one mononucleosome (Figures 3C, inset, S3A, and S3B). We note that even when the antibody binding efficiency was similar in the absence and presence of nuclear extract, we cannot fully exclude some underestimation in the nucleosome numbers, in particular for the larger clutches. Nevertheless, this underestimation should not affect the relative comparison among the different cell types.

We next used the calibration curve to estimate the median number of nucleosomes per clutch (Figure 3D). Clutches in hFbs comprised a median of ~ 8 nucleosomes whereas this number decreased to ~ 2 nucleosomes after TSA treatment (Figure 3D, left). mESCs cultured in sLif constituted a heterogeneous population compared to other mESCs, consisting of cells with a median of ≥ 4.5 nucleosomes (type 1 mESCs, corresponding to

22 ± 2 localizations) and cells with a median of < 4.5 nucleosomes per clutch (type 2 mESCs, corresponding to 17 ± 2 localizations) (Figure 3D, right; Extended Experimental Procedures). mNPCs were also heterogeneous and had clutches with on average a larger number of nucleosomes (~ 6 , Figure 3D, right). The number of nucleosomes per clutch was less variable in mESCs cultured in 2iLif, mESC^{Tcf3^{-/-}}, and mESC^{H1tKO} (median of ~ 3 , ~ 3.5 , and ~ 2 , respectively) (Figure 3D, right). These results indicate that nucleosomes are assembled together in smaller clutches in pluripotent cells and in increasing numbers in differentiated cells. Furthermore, clutch size drastically changes upon chromatin decondensation after TSA treatment.

hFbs had more densely compacted nucleosome clutches compared to TSA-hFbs (Figure 3E) as determined from the median nucleosome density (number of nucleosomes per unit area). Nucleosome density was likewise higher for mNPCs and mESCs cultured in sLif with respect to mESCs cultured in 2iLif, mESC^{Tcf3^{-/-}} and mESC^{H1tKO} (Figure 3F). Therefore, nucleosome density is in general low in pluripotent cells and nucleosome compaction increases upon differentiation.

Clutch Size Correlates with the Pluripotency Grade of Human-Induced Pluripotent Stem Cells

Next, we aimed to study whether the number of nucleosomes per clutch could be predictive of the pluripotency grade in human-induced pluripotent stem cell (hiPSCs) clones, as defined by their gene expression profile and propensity to differentiate. hiPSCs were generated from hFbs and characterized using standard methods (Figures S4A–S4D). The hiPSC clone 13 and 8 were both pluripotent since they were AP-positive and expressed the stem cell markers TRA1-60, SSEA4, Oct4, Sox2, and Nanog. However, while the hiPSC clone 13 formed embryoid bodies, which differentiated into the three germ layers, and generated large and fully differentiated teratomas in mice, the hiPSC clone 8 did not form the ectoderm layer from the embryoid bodies and it generated very small undifferentiated teratomas in vivo (Figures S4A–S4D). Furthermore, the Oct4 expression level of single cells in the hiPSC clone 8 was 14-fold lower compared to hiPSC clone 13 (Figure S4B). Therefore, the pluripotency grade of clone 13 was higher compared to clone 8. To rank the pluripotency grade of all hiPSC clones in a more quantitative manner, we used the gene card technology that gives a pluripotency score based on expression level of stemness genes and differentiation propensity compared to a reference set of formerly characterized human embryonic stem cell (hESC) and hiPSC lines (Bock et al., 2011). The gene card results agreed with the classical characterization of clones 8 and 13 and allowed quantitative ranking of the remaining hiPSC clones in order of pluripotency grade (Figure S4E).

The median number of localizations quantified from STORM images (Figure 4A) showed statistically significant differences among the different clones and gradually increased passing from the hiPSCs clone 13 to 8. The calibration curve was used to deduce the median number and density of nucleosomes inside clutches in each hiPSC clone (Figures 4B and 4C). There was a remarkable agreement between the pluripotency score obtained from the gene card and the clutch size

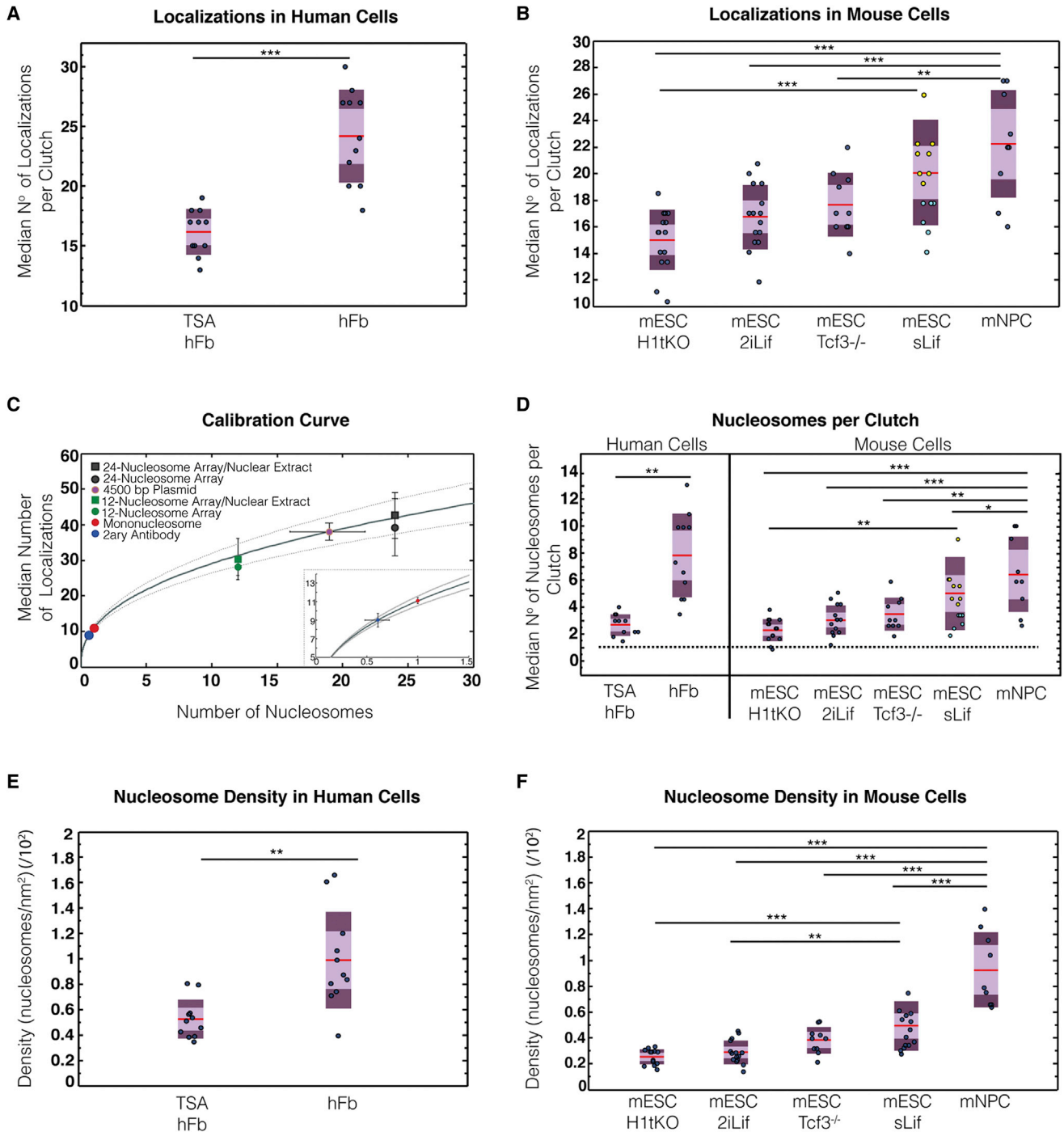


Figure 3. The Number of Nucleosomes Inside Clutches Correlates with Cellular State

(A and B) Box plots showing the median number of H2B localizations per clutch in hFbs (n = 11 cells), TSA-hFbs (n = 11 cells) (A), in different mESCs (n = 15, 15, 10, and 14 cells, respectively, from left to right), and in mNPCs (n = 9 cells). (B) mESC sLif cells are color coded as type 1 containing a median of 22 ± 2 localizations (yellow) (n = 8 cells) and type 2 containing a median of 17 ± 2 localizations (cyan) (n = 6 cells).

(C) Calibration curve to deduce the median number of nucleosomes per clutch. The median number of localizations per mononucleosome (red circle), 12- (green circle) and 24-nucleosome array (black circle) labeled and imaged in vitro, 12- (green square) and 24-nucleosome array (black square) labeled and imaged in the presence of a nuclear extract were used to generate the calibration curve. The gray line is the fit for the data in the presence of nuclear extract to a power law $y = ax^b$ with $a = 11 \pm 3$ and $b = 0.41 \pm 0.15$. Errors correspond to 95% confidence bounds. The dotted lines represent 68% confidence interval. Purple circle is data from a 4,500 base pair (bp) plasmid assembled into nucleosome-arrays with an expected number of ~ 20 nucleosomes per array. Blue circle is data from

(legend continued on next page)

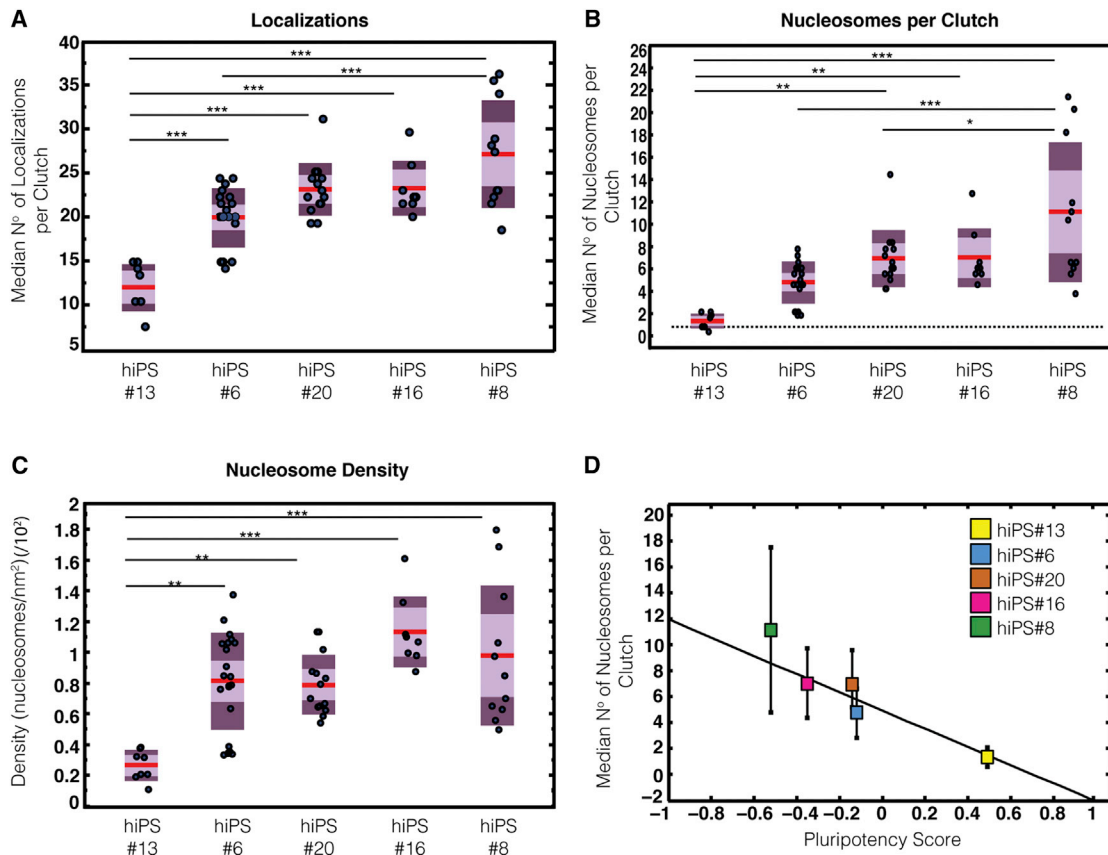


Figure 4. Clutch Size Correlates with Pluripotency Grade in Human-Induced Pluripotent Stem Cells Clones

(A) Box plots showing the median number of H2B localizations per clutch in different human-induced pluripotent stem cell (hiPSCs) clones ($n = 8, 20, 14, 8,$ and 11 cells from left to right, respectively, from multiple imaging experiments [minimum of 3]).

(B) Box plots showing the median number of nucleosomes per clutch in the different hiPSCs. The dotted line corresponds to one nucleosome.

(C) Box plots showing the median density of nucleosomes per clutch in the different hiPSCs.

(D) Pluripotency score of the different hiPSCs obtained from the gene card plotted against the median number of nucleosomes. Error bars indicate SDs. For black dots, lines, box plot colors and statistics in (A)–(C) see description in the legend of Figure 3.

See also Figure S4.

(Figure 4D), (analysis showed $r = -0.94$ indicating high level of anticorrelation, i.e., low number of nucleosomes per clutch for high pluripotency score and vice versa). Indeed, the hiPSC clone 13, which showed high propensity to differentiate and a high pluripotency score, had low density clutches with a median number of only 1 nucleosome, while clutch size and density increased progressively with the decreased pluripotency score (Figures 4B–4D).

Larger Clutches Have Higher Levels of H1 and Lower Levels of RNA Polymerase II

The arrangement of nucleosomes in small clutches with lower compaction could potentially facilitate the binding of transcription factors, polymerases, and other proteins to the DNA, which should be more accessible in regions containing smaller clutches. The higher compaction of the nucleosomes within larger clutches, on the other hand, should restrict DNA

fluorophore-labeled secondary antibody alone. Inset shows the first part of the curve containing the secondary antibody and the mononucleosomes. Error bars correspond to SDs.

(D) Box plots showing the median number of nucleosomes per clutch in hFBs, TSA-hFBs, in the different types of mESCs and in mNPCs. The dotted line corresponds to one nucleosome.

(E and F) Box plots showing the median density of nucleosomes per clutch in hFBs, TSA-hFBs (E) in the different types of mESCs and mNPCs (F). For (A), (B), and (D–F) each black dot shows the median number of nucleosomes obtained per individual nucleus from multiple imaging experiments (minimum of 3). The red line is the median for the entire population of nuclei analyzed for that cell type. The light magenta region corresponds to the SE and the dark magenta region to the SD. Statistical significance between the different cell types was determined using one-way ANOVA. The stars indicate p values according to * ($p < 0.05$), ** ($p < 0.01$), and *** ($p < 0.001$).

See also Figure S3.

accessibility and should be aided by the presence of linker histone protein H1, which is known to be involved in nucleosome compaction and is enriched in heterochromatin (Fan et al., 2005; Woodcock et al., 2006). Thus, to evaluate differences in the heterochromatin content of clutches and their accessibility to RNA Polymerase II (PolII), we performed multi-color STORM imaging of H2B with histone H1 and of H2B with PolII.

H1 was more enriched at the nuclear periphery of hFbs where heterochromatin is more abundant (Meister and Taddei, 2013) (Figure 5A). A higher percentage of H2B co-localized with H1 in hFbs ($61\% \pm 11\%$) compared to TSA-hFbs ($42\% \pm 6\%$) ($p = 0.028$) as is also evident in the zoomed images (Figures 5A and 5B). For both hFbs and TSA-hFbs, the number of H1 localizations in the clutches increased with the number of H2B localizations (Figures 5C and S5A). In mESCs cultured in sLif, $\sim 54\% \pm 2\%$ of H2B co-localized with H1 and the number of H1 localizations also increased with the number of H2B localizations (Figure S5B). As expected, mESCs^{H1¹KO} contained much lower amount of H1 (Figure S5C) and only $\sim 35\% \pm 4\%$ of H2B co-localized with H1 ($p = 0.0057$). Despite the low amount of H1 in these cells, the same trend was observed, i.e., the number of H1 localizations was increased in clutches with an increasing number of H2B localizations (Figure S5B). These results overall suggest that the number of H1 histones correlates with the number of nucleosomes inside the clutches.

Since the largest clutches containing high amounts of H1 were also the more densely compacted ones (Figures 3E and 3F) we hypothesized that these might correspond to the ‘closed’ heterochromatin regions. To test this hypothesis we used an anti-CREST antibody to recognize specific centromeric proteins. Centromeres are known to include heterochromatin (Meister and Taddei, 2013). CREST positive regions co-localized with the large clutches (Figure 5D) containing on average 1.3-fold higher number of H2B localizations compared to the global median ($p = 0.014$) (Figure S5D). A similar analysis was performed in mESCs expressing a TALE-mClover that accumulates at pericentromeric regions in these cells (Miyanari et al., 2013). mClover positive regions once again correlated with large clutches (Figure 5E) and clutches that overlapped with TALE-mClover contained on average 2.2-fold higher number of H2B localizations compared to the global median ($p = 0.0002$) (Figure S5E).

Next we analyzed PolII and H2B multi-color STORM images of hFbs and TSA-hFbs. In both cases, PolII was partially interspersed and partially co-localized with the nucleosome clutches (Figure 6A and zooms). PolII-H2B nnds peaked at ~ 40 nm (Figure 6B). We rationalized that the DNA within clutches having fewer nucleosomes should be more accessible and therefore PolII should be closest to the small clutches. To test this hypothesis, we analyzed the number of H2B localizations within clutches as a function of the nnds between PolII and H2B, restricting the analysis to nnds below 70 nm, which corresponds to the maximum PolII cluster size plus the maximum clutch size. For both hFbs and TSA-hFbs, the nnds between PolII and H2B were shorter for smaller clutches, indicating that PolII was indeed closer to the smaller clutches with few nucleosomes (Figure 6C). These results indicate that PolII can access small clutches, which likely form the ‘open’ chromatin fiber arrangement of transcribed chromatin regions.

The DNA Fiber Is Not Fully Occupied with Nucleosomes

The organization of nucleosomes in discrete, spatially separated clutches implies that nucleosome-depleted regions likely exist in the chromatin fiber. We hypothesized that these regions might be due to removal of nucleosomes in between nucleosome-rich regions or to variations in the length of the linker-DNA between subsequent nucleosomes. Coarse-grained computer simulations of nucleosome spatial arrangement were performed, using a simplistic model that considers a minimum number of parameters (Extended Experimental Procedures; Figures 7A–7C). In this model, we simulated either random removal of nucleosomes with a given probability (NR Model; Extended Experimental Procedures; Figure 7D) or variations in the average length of the linker-DNA (LL Model, Extended Experimental Procedures; Figure 7E) or potential effects of incomplete labeling (Extended Experimental Procedures; Figures S6A and S6B).

Synthetic STORM images of the nucleosomes along the DNA fiber (Figures 7F and S6A) were generated by assigning to each nucleosome a given number of localizations based on the in vitro calibration results (Extended Experimental Procedures; Figure S3B). The synthetic STORM images at different nucleosome occupancy levels (Figure 7F) showed striking resemblance to the experimental images. The median number of localizations, area, and nnds of the nucleosome clutches were determined using identical analysis parameters as before and plotted as a function of nucleosome occupancy (Figure 7G).

Both the NR and LL models intersected the experimental values of the number of localizations and the clutch nnds at $\sim 57\%$ and $\sim 45\%$ occupancy for the hFbs and TSA-hFbs, respectively (Figure 7G, top and middle). For TSA-hFb, the NR model intersected the experimental value of the clutch area at a similar occupancy level (45%) whereas the LL model intersected it at a much lower occupancy level (34%) (Figure 7G, bottom). For hFbs, the NR model intersected the experimental value of clutch area at a slightly higher occupancy level than those obtained from the other two parameters (60%) whereas the LL model intersected this value at a slightly lower occupancy level (52%) (Figure 7G, bottom).

In the case of labeling efficiency simulations, the three measured experimental parameters could not be simultaneously reproduced at any given labeling efficiency for hFbs and TSA-hFbs (Figure S6B), indicating that poor labeling efficiency alone cannot explain the experimental observations. However, nucleosome depletion in combination with incomplete labeling can lead to the observed results, shifting the nucleosome occupancy to higher values (Figure S6C). Regardless of the labeling efficiency, nucleosome occupancy was higher in hFbs compared to TSA-hFbs. The simulation results could reproduce both the median values observed for the experimental data as well as the full experimental distributions, with the best fit for the NR model corresponding to 75% labeling efficiency for both hFb (60% occupancy) and TSA-hFb (48% occupancy) (Figures S6D–S6F).

Taken altogether, these results indicate that linker length variations do not play a major role in generating nucleosome poor regions in TSA-hFbs since all three measured parameters of the experimental data could not be recapitulated with this model. In the case of hFbs, combination of nucleosome removal and

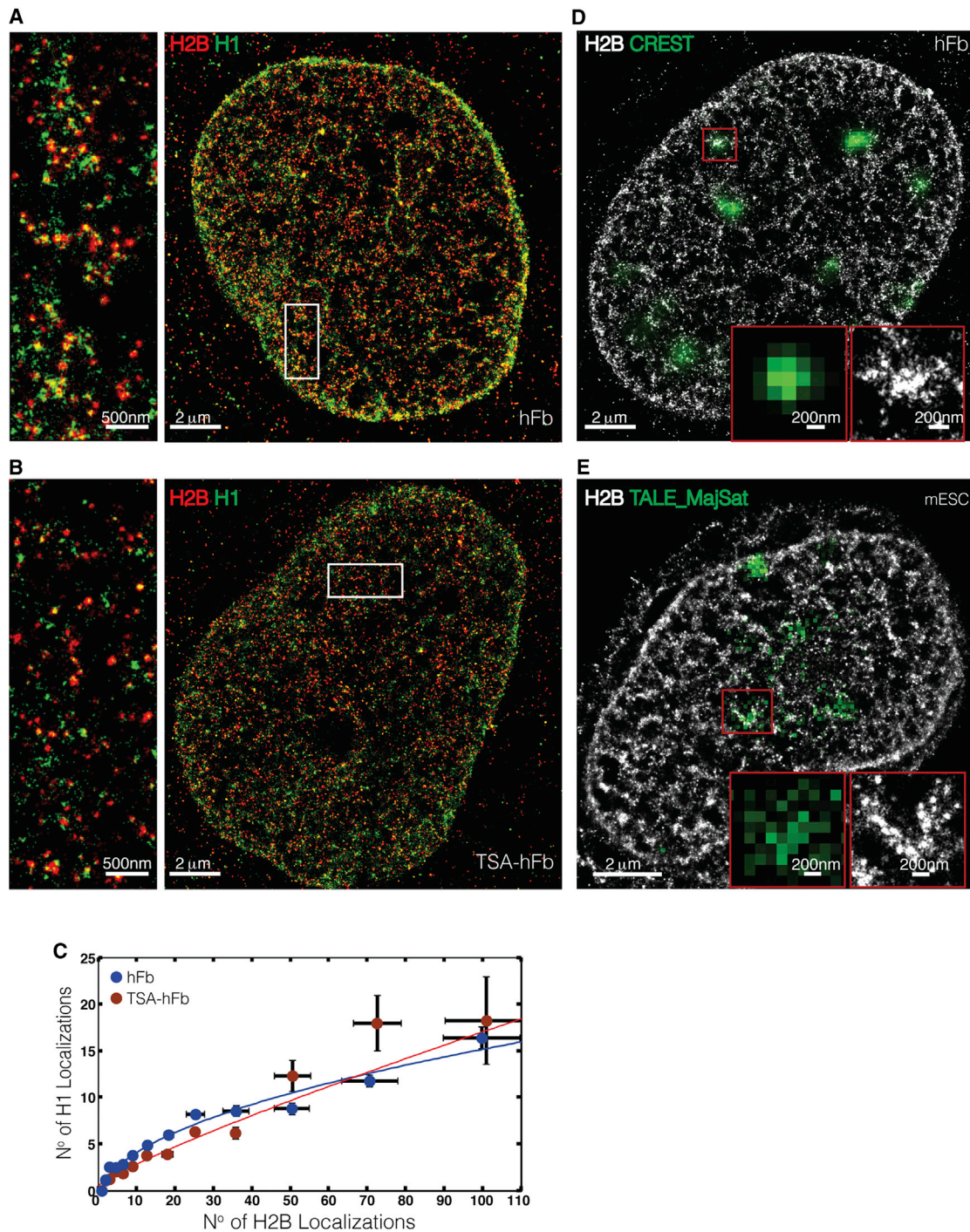


Figure 5. The Linker Histone H1 Increases in Large Clutches and These Correlate with Heterochromatin Markers

(A and B) Representative STORM images showing H2B (red) and H1 (green) in hFb ($n = 4$ cells) (A) and TSA-hFb ($n = 4$ cells) (B). Higher zooms of the regions inside white rectangles are shown next to each nucleus.

(C) Plot showing the number of H2B (x axis) and H1 (y axis) localizations inside clutches for which these two histones showed colocalization. Error bars in x axis indicate SDs and in y axis indicate SEs. The trend lines are polynomial fits intended as a guide to the eye.

(D) Representative STORM image of H2B (gray) overlaid with the conventional fluorescence image of anti-CREST antibody (green) which recognizes centromeric proteins in hFbs ($n = 6$ cells). Inset shows a zoomed in region of the red square.

(E) Representative STORM image of H2B (gray) overlaid with the conventional fluorescence image of TALE-mCjlover that recognizes the major satellite of pericentromeric regions (TALE_MajSat) (green) in mESC sLif ($n = 16$ cells). Inset shows a zoomed in region of the red square.

See also [Figure S5](#).

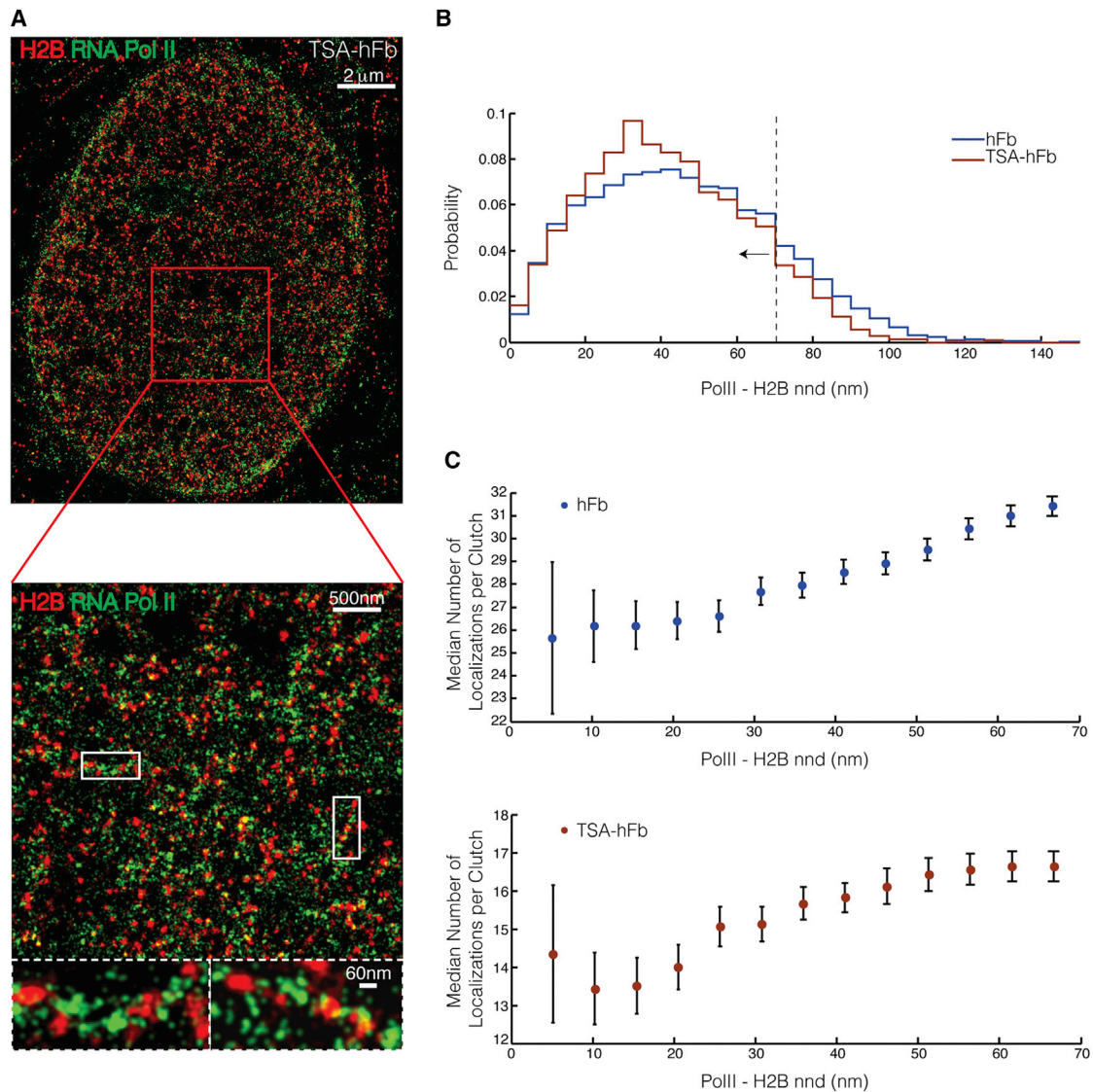


Figure 6. RNA Polymerase II Associates with the Small Clutches

(A) Representative STORM image showing H2B (red) and RNA polymerase II (PolII) (green) in TSA-hFb. Progressive zooms of the regions inside white rectangles are shown below the image of the nucleus.

(B) Plot showing the distribution of nnds between H2B and PolII in hFb (blue) ($n = 5$ cells) and TSA-hFb (red) ($n = 3$ cells). The dashed line at 70 nm shows the distance cut-off used for the analysis in (C) corresponding to maximum clutch size plus maximum PolII cluster size.

(C) Plot showing the median number of H2B localizations within clutches as a function of the nnds (up to a maximum nnd of 70 nm) between PolII and H2B for hFb (blue) and TSA-hFb (red). Error bars indicate SEs.

linker-DNA length modifications likely plays a role in generating the nucleosome-depleted regions.

DISCUSSION

Chromatin organization and structure in interphase nuclei is important for gene function and activity, therefore it is an area of intense investigation (Wendt and Grosveld, 2014). Electron microscopy (EM) and more recently cryo-EM (Song et al., 2014) have provided invaluable insight into nucleosome organization in vitro. However, in vitro studies cannot determine if the organi-

zation observed is prevalent in vivo in intact nuclei. The structure of chromatin has also been subject to a number of in vivo studies (Fussner et al., 2011a). Although these previous methods have provided key information, they are accompanied with major drawbacks such as harsh sample preparation, lack of molecular specificity and/or low resolution, such that a clear picture on the organization of nucleosomes along the chromatin fiber in living cells has been lacking so far. Here, we have come closer than ever to visualize the native structure of the chromatin fiber by dissecting at nanoscale resolution the organization of nucleosomes in intact nuclei and in single cells. STORM imaging revealed that

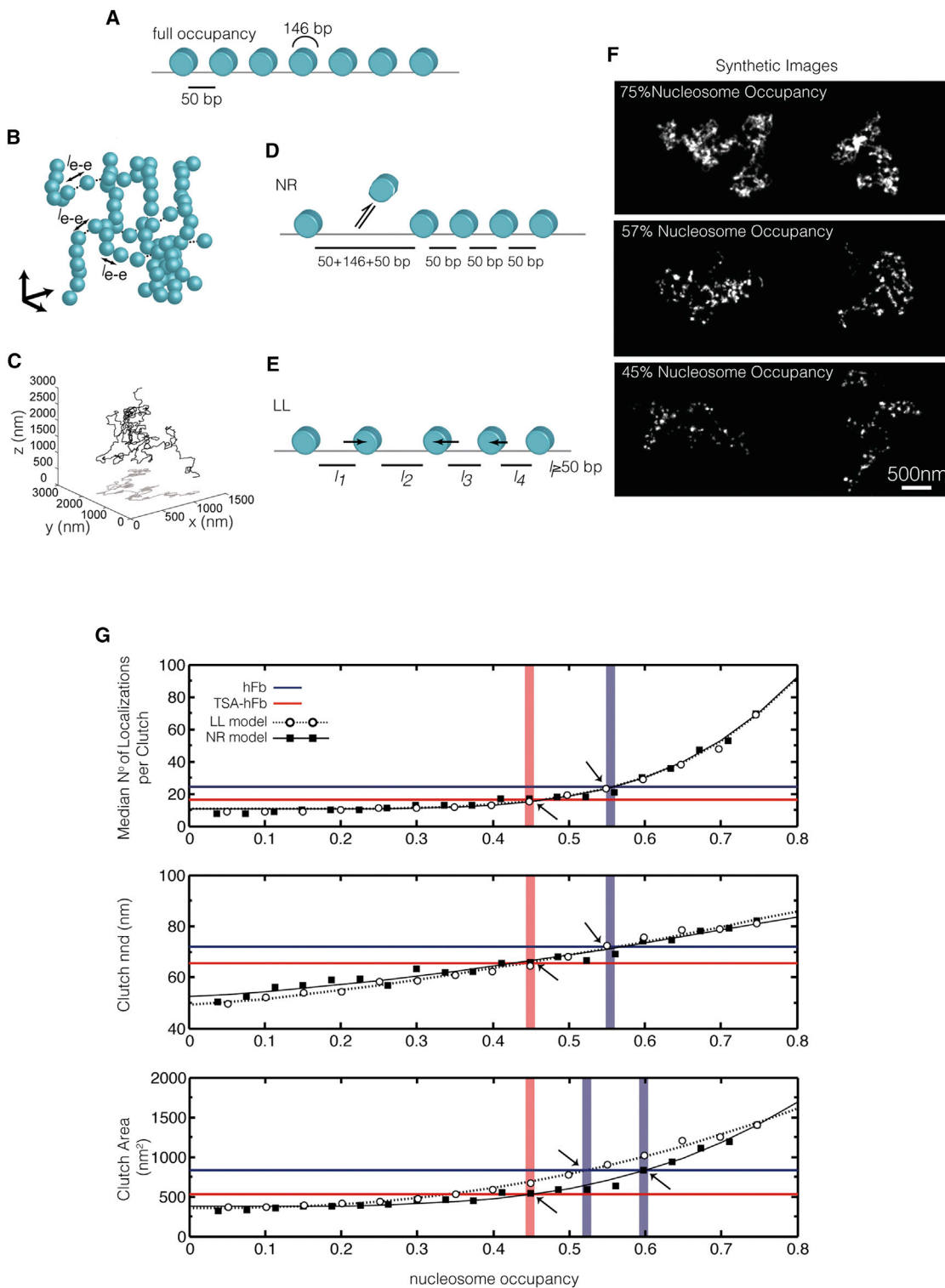


Figure 7. Computer Simulations of Nucleosome Occupancy

(A) Nucleosomes (light blue) are initially arranged at regular intervals of 50 bp (experimentally determined linker-DNA length) on the DNA fiber, (full occupancy, which in reality corresponds to 75% of DNA occupied with nucleosomes). DNA (146 bp) wraps around each nucleosome.

(B) A 3D DNA fiber arrangement is generated by positioning nucleosomes according to a Gaussian chain model with end-to-end distances (l_{e-e}) calculated according to the worm like chain model (WLM) for a polymer with a persistence length of 150 bp (experimentally determined persistence length of DNA).

(legend continued on next page)

(1) nucleosomes do not form a highly ordered organization but rather arrange into discrete groups, the clutches, of various sizes and densities, which are interspaced by nucleosome-depleted regions; (2) there is a striking correlation between spatial distribution, size, and compaction of nucleosome clutches and cell pluripotency; (3) ground-state stem cells have low-density clutches containing on average only a few nucleosomes; and (4) large clutches with higher nucleosome compaction corresponds to heterochromatin and include more H1, whereas the small clutches with lower nucleosome compaction correspond to active chromatin regions since they are associated to RNA Polymerase II.

While the heterogeneity of the nucleosome clutches argues against the existence of highly ordered structures such as the 30-nm fiber, it is still possible that nucleosomes maintain an ordered organization inside the clutches. Nevertheless, our simple *in silico* model can reconstruct “nucleosome-rich” and “nucleosome-depleted” regions that recapitulate the experimental results without invoking the existence of a 30-nm fiber. Therefore, our data indicate that an ordered structure is not strictly required for the observed organization of nucleosomes.

In this work, we have discovered an important feature of embryonic stem cells, *i.e.*, their characteristic nucleosome organization along the chromatin fiber. Furthermore, we have revealed a striking correlation between naive pluripotent state and nucleosome arrangement, which was made possible by the direct visualization of nucleosomes at nanoscale resolution. We found that drugs, such as TSA, which trigger massive epigenome modifications and facilitate somatic cell reprogramming (Lluis and Cosma, 2013), induce a spatial rearrangement of nucleosome clutches and modify their density. These structural modifications can potentially facilitate the maintenance of pluripotency as well as the establishment of an induced pluripotent state.

Chromatin of mESCs is hyper-dynamic, shows increased transcriptional activity and contains a high number of DNase I hypersensitivity sites (Efroni *et al.*, 2008; Fussner *et al.*, 2011b; Meshorer *et al.*, 2006; Stergachis *et al.*, 2013). These features, associated with “open” chromatin, are consistent with the existence of small, low-density clutches in mESCs. Here, by the direct visualization of nucleosomes we can now identify “open” and “closed” chromatin as small, low-density and large, high-density nucleosome clutches, respectively, and relate clutch size to cellular state. Clutch size could not only report on heterogeneities in a given mESC population but importantly, it also highly correlated with the pluripotency grade of hiPSCs.

Pluripotency grade of different hiPSCs clones can therefore potentially be characterized and compared at the single cell level using this method. Overall, these results open up exciting possibilities for identifying stem cell state simply by analyzing nucleosome arrangement. It will also be very interesting to determine whether differences in the clutches exist between different cell types such as cancer and normal cells, and if so, whether the clutch size can also be used as a diagnostic marker for cancer cell identification and consequent follow up therapies, or to identify rare subpopulations of stem/precursor cells within a specific tissue.

Nucleosome occupancy is critical for biological function since there should be a reservoir of DNA that is ready to be decoded by transcription factors and RNA polymerases. Population studies have measured an average linker-DNA length of around 50 bp between subsequent nucleosomes (Kornberg, 1977; Valouev *et al.*, 2011; Widom, 1992), which would correspond to DNA occupancy of ~75%. Here, we estimate an occupancy level of ~60% in hFbs, which might be slightly underestimated since our model does not take into account that not all nucleosomes may be labeled inside the large clutches. Our result comes very close to the occupancy level measured in genome-wide studies (Jiang and Pugh, 2009; Struhl and Segal, 2013). However, it is difficult to directly compare genome-wide chromatin immunoprecipitation (ChIP) or micrococcal nuclease (MNase) studies with STORM imaging to extract information on nucleosome number and their localization on DNA since the former methods are based on population studies and have a resolution in the range of hundreds of nanometers, whereas STORM reveals nucleosomes in single cells with much higher resolution (10–20 nm). In the future, it will be exciting to visualize both DNA and nucleosomes by STORM at specific gene loci, which may enable better comparison of the clutch data with the ChIP analysis.

EXPERIMENTAL PROCEDURES

Full details of the experimental procedures and analyses are provided online in the [Extended Experimental Procedures](#).

Sample Preparation and STORM Imaging

Cells were fixed with methanol-ethanol (1:1) at -20°C for 6 min unless otherwise stated and immunostained with appropriate primary and secondary antibodies. Secondary antibodies were labeled with activator-reporter dye pairs (Alexa Fluor 405-Alexa Fluor 647) for STORM imaging. All imaging experiments were carried out with a commercial STORM microscope system from Nikon Instruments (NSTORM). Laser light at 647 nm was used for

(C) The resulting DNA fiber configuration is projected onto 2D space.

(D) In the nucleosome removal (NR) model, nucleosomes are removed from the DNA with a given probability ranging from 0 to 0.95. When a nucleosome is removed, the linker-DNA length between the neighboring nucleosomes increases by 146 bp.

(E) In the linker length (LL) model the linker-DNA lengths (l_i) between subsequent nucleosomes are drawn from normal distributions whose averages are varied from 50 bp to 3,000 bp.

(F) Examples of synthetic STORM images obtained from the simulated arrangement of nucleosomes at 75%, 57%, and 45% nucleosome occupancy.

(G) Comparison of simulation results for the NR- (black squares and solid line) and LL-Models (white circles and dotted line) to experimental data for hFbs (horizontal blue line) and TSA-hFbs (horizontal red line) at different levels of nucleosome occupancy (x axis). The comparison is made for the number of localizations per clutch (upper), nnds of clutches (middle) and clutch area (lower). The vertical thick blue lines and black arrows show the nucleosome occupancy values for which the simulation results of the different models intersect the experimental data for the hFbs. Similarly, the vertical thick red lines and black arrows show the nucleosome occupancy values for which the simulation results intersect the experimental data for the TSA-hFbs. Trend lines are polynomial fits.

See also [Figure S6](#).

exciting Alexa Fluor 647, and laser light at 405 nm was used for activating it via an activator dye (Alexa Fluor 405)-facilitated manner. For all single color H2B imaging experiments, activation laser (405 nm) power was increased over time in an identical way according to Table S1. For dual color imaging, a second activator-reporter dye pair (Cy3-Alexa Fluor 647) and an additional activation laser at 560 nm was used. The emitted light was collected by an oil immersion 100 \times , 1.49 NA objective, filtered by an emission filter (ET705/72 m), and imaged onto an electron multiplying charge coupled device (EMCCD) camera at an exposure time of 15 ms per frame. For live-cell imaging, cells were transfected with H2B-mEos2 or H2B-PAmCherry. Laser light at 405 nm was used to photoactivate the fluorescent proteins and laser light at 560 nm was used to excite the photoactivated forms. The fluorescence emission was filtered with an emission filter (BP 605/52) and recorded with an exposure time of 50 ms per frame.

Data Analysis

STORM images were analyzed using custom-written software (Insight3, provided by Bo Huang, University of California, San Francisco) by fitting the fluorophore images in each frame to a simple Gaussian to determine x-y coordinates.

For cluster quantification, x-y localization lists were binned to construct discrete localization images with pixel size of 10 nm. These were convoluted with a square kernel (5×5 pixels²) to obtain density maps and transformed into binary images by applying a constant threshold. x-y coordinates in the binary image were grouped into clusters using a distance-based algorithm. Cluster sizes were calculated as the SD of x-y coordinates from the relative cluster centroid.

SUPPLEMENTAL INFORMATION

Supplemental Information includes Extended Experimental Procedures and six figures and can be found with this article online at <http://dx.doi.org/10.1016/j.cell.2015.01.054>.

AUTHOR CONTRIBUTIONS

M.P.C., M.L., M.A.R., C.M., and M.F.G.-P. designed the experiments and data analysis. M.A.R. performed experiments and data analysis. C.M. wrote software and performed data analysis. M.P.C., M.L., M.A.R., C.M., and M.F.G.-P. wrote the manuscript. M.P.C., M.L., and M.F.G.-P. supervised the project.

ACKNOWLEDGMENTS

We thank A. Skoultchi (Albert Einstein College of Medicine), S. Grigoryev (Penn State Hershey Cancer Institute), T. Misgeld (TUM, Munich), X. Zhuang (Harvard University) and J. Ries (European Molecular Biology Laboratory [EMBL], Heidelberg) for providing reagents and cell lines, B. Huang (University of California, San Francisco [UCSF]) for Insight3 STORM analysis software, L. Batlle Morera (Center for Genomic Regulation [CRG], Barcelona) for helping in hiPSC generation, J. Font Mateu (CRG, Barcelona) for technical suggestions on in vitro polynucleosome, F. Sottile (CRG, Barcelona) for cloning the H2B-mEos2 plasmid. We thank M. Beato, C. di Vona, G. Filion, T. Graf, B. Lehner, M. Marti-Renom, M. Mendoza, J. Sharpe, J. Solon and J. Valcarcel (CRG, Barcelona), E. Meshorer (Hebrew University of Jerusalem), A. Oddone and J. Otterstrom (Institute of Photonic Sciences [ICFO], Barcelona), and X. Zhuang (Harvard University) for critical reading of the manuscript and helpful discussions. We acknowledge the ICFO Super-resolution Light Nanoscopy (SLN) facility, the ICFO Nikon Center of Excellence in STORM, the CRG microscopy facility and the EMBL electron microscopy core facility. We thank E. Sahagún Alonso (Scixel) and A. Hirschmann (ICFO) for help with the graphical abstract. The research leading to these results was supported in part by the Fundació Cellex Barcelona (M.L.), the System's Microscopy Network of Excellence consortium (call identifier FP-7-HEALTH.2010.2.1.2.2 to M.L.), by the European Union Seventh Framework Programme under the European Research Council grants 337191-MOTOS to M.L. and 242630-RERE to M.P.C., a Human Frontier Science Program (HFSP) grant (M.P.C.), and MAT2011-22887

(M.F.G.-P). This article reflects only the author's views and the Union is not liable for any use that may be made of the information contained therein.

Received: June 4, 2014

Revised: October 10, 2014

Accepted: January 16, 2015

Published: March 12, 2015

REFERENCES

- Bock, C., Kiskinis, E., Verstappen, G., Gu, H., Boulting, G., Smith, Z.D., Ziller, M., Croft, G.F., Amoroso, M.W., Oakley, D.H., et al. (2011). Reference Maps of human ES and iPS cell variation enable high-throughput characterization of pluripotent cell lines. *Cell* 144, 439–452.
- Bohn, M., Diesinger, P., Kaufmann, R., Weiland, Y., Müller, P., Gunkel, M., von Ketteler, A., Lemmer, P., Hausmann, M., Heermann, D.W., and Cremer, C. (2010). Localization microscopy reveals expression-dependent parameters of chromatin nanostructure. *Biophys. J.* 99, 1358–1367.
- Cahan, P., and Daley, G.Q. (2013). Origins and implications of pluripotent stem cell variability and heterogeneity. *Nat. Rev. Mol. Cell Biol.* 14, 357–368.
- Clausell, J., Happel, N., Hale, T.K., Doenecke, D., and Beato, M. (2009). Histone H1 subtypes differentially modulate chromatin condensation without preventing ATP-dependent remodeling by SWI/SNF or NURF. *PLoS ONE* 4, e0007243.
- Cole, M.F., Johnstone, S.E., Newman, J.J., Kagey, M.H., and Young, R.A. (2008). Tcf3 is an integral component of the core regulatory circuitry of embryonic stem cells. *Genes Dev.* 22, 746–755.
- Dani, A., Huang, B., Bergan, J., Dulac, C., and Zhuang, X. (2010). Superresolution imaging of chemical synapses in the brain. *Neuron* 68, 843–856.
- Duricic, N., Cuervo, L.L., and Lakadamyali, M. (2014). Quantitative super-resolution microscopy: pitfalls and strategies for image analysis. *Curr. Opin. Chem. Biol.* 20, 22–28.
- Efroni, S., Dutttagupta, R., Cheng, J., Dehghani, H., Hoepfner, D.J., Dash, C., Bazett-Jones, D.P., Le Grice, S., McKay, R.D., Buetow, K.H., et al. (2008). Global transcription in pluripotent embryonic stem cells. *Cell Stem Cell* 2, 437–447.
- Fan, Y., Nikitina, T., Zhao, J., Fleury, T.J., Bhattacharyya, R., Bouhassira, E.E., Stein, A., Woodcock, C.L., and Skoultchi, A.I. (2005). Histone H1 depletion in mammals alters global chromatin structure but causes specific changes in gene regulation. *Cell* 123, 1199–1212.
- Finch, J.T., and Klug, A. (1976). Solenoidal model for superstructure in chromatin. *Proc. Natl. Acad. Sci. USA* 73, 1897–1901.
- Fussner, E., Ching, R.W., and Bazett-Jones, D.P. (2011a). Living without 30nm chromatin fibers. *Trends Biochem. Sci.* 36, 1–6.
- Fussner, E., Djuric, U., Strauss, M., Hotta, A., Perez-Iratxeta, C., Lanner, F., Dilworth, F.J., Ellis, J., and Bazett-Jones, D.P. (2011b). Constitutive heterochromatin reorganization during somatic cell reprogramming. *EMBO J.* 30, 1778–1789.
- Fussner, E., Strauss, M., Djuric, U., Li, R., Ahmed, K., Hart, M., Ellis, J., and Bazett-Jones, D.P. (2012). Open and closed domains in the mouse genome are configured as 10-nm chromatin fibres. *EMBO Rep.* 13, 992–996.
- Grigoryev, S.A., Arya, G., Correll, S., Woodcock, C.L., and Schlick, T. (2009). Evidence for heteromorphic chromatin fibers from analysis of nucleosome interactions. *Proc. Natl. Acad. Sci. USA* 106, 13317–13322.
- Jiang, C., and Pugh, B.F. (2009). Nucleosome positioning and gene regulation: advances through genomics. *Nat. Rev. Genet.* 10, 161–172.
- Joti, Y., Hikima, T., Nishino, Y., Kamada, F., Hihara, S., Takata, H., Ishikawa, T., and Maeshima, K. (2012). Chromosomes without a 30-nm chromatin fiber. *Nucleus* 3, 404–410.
- Kamakaka, R.T., and Biggins, S. (2005). Histone variants: deviants? *Genes Dev.* 19, 295–310.

- Kornberg, R.D. (1977). Structure of chromatin. *Annu. Rev. Biochem.* *46*, 931–954.
- Lluis, F., and Cosma, M.P. (2013). Resetting epigenetic signatures to induce somatic cell reprogramming. *Cell. Mol. Life Sci.* *70*, 1413–1424.
- Lluis, F., Ombrato, L., Pedone, E., Pepe, S., Merrill, B.J., and Cosma, M.P. (2011). T-cell factor 3 (Tcf3) deletion increases somatic cell reprogramming by inducing epigenome modifications. *Proc. Natl. Acad. Sci. USA* *108*, 11912–11917.
- Luger, K., Mäder, A.W., Richmond, R.K., Sargent, D.F., and Richmond, T.J. (1997). Crystal structure of the nucleosome core particle at 2.8 Å resolution. *Nature* *389*, 251–260.
- Marks, H., Kalkan, T., Menafra, R., Denissov, S., Jones, K., Hofemeister, H., Nichols, J., Kranz, A., Stewart, A.F., Smith, A., and Stunnenberg, H.G. (2012). The transcriptional and epigenomic foundations of ground state pluripotency. *Cell* *149*, 590–604.
- Matsuda, A., Shao, L., Boulanger, J., Kervrann, C., Carlton, P.M., Kner, P., Agard, D., and Sedat, J.W. (2010). Condensed mitotic chromosome structure at nanometer resolution using PALM and EGFP- histones. *PLoS ONE* *5*, e12768.
- Meister, P., and Taddei, A. (2013). Building silent compartments at the nuclear periphery: a recurrent theme. *Curr. Opin. Genet. Dev.* *23*, 96–103.
- Meshorer, E., Yellajoshula, D., George, E., Scambler, P.J., Brown, D.T., and Misteli, T. (2006). Hyperdynamic plasticity of chromatin proteins in pluripotent embryonic stem cells. *Dev. Cell* *10*, 105–116.
- Miyazari, Y., Ziegler-Birling, C., and Torres-Padilla, M.E. (2013). Live visualization of chromatin dynamics with fluorescent TALEs. *Nat. Struct. Mol. Biol.* *20*, 1321–1324.
- Nishino, Y., Eltsov, M., Joti, Y., Ito, K., Takata, H., Takahashi, Y., Hihara, S., Frangakis, A.S., Imamoto, N., Ishikawa, T., and Maeshima, K. (2012). Human mitotic chromosomes consist predominantly of irregularly folded nucleosome fibres without a 30-nm chromatin structure. *EMBO J.* *31*, 1644–1653.
- Rust, M.J., Bates, M., and Zhuang, X. (2006). Sub-diffraction-limit imaging by stochastic optical reconstruction microscopy (STORM). *Nat. Methods* *3*, 793–795.
- Song, F., Chen, P., Sun, D., Wang, M., Dong, L., Liang, D., Xu, R.M., Zhu, P., and Li, G. (2014). Cryo-EM study of the chromatin fiber reveals a double helix twisted by tetranucleosomal units. *Science* *344*, 376–380.
- Stergachis, A.B., Neph, S., Reynolds, A., Humbert, R., Miller, B., Paige, S.L., Vernot, B., Cheng, J.B., Thurman, R.E., Sandstrom, R., et al. (2013). Developmental fate and cellular maturity encoded in human regulatory DNA landscapes. *Cell* *154*, 888–903.
- Struhl, K., and Segal, E. (2013). Determinants of nucleosome positioning. *Nat. Struct. Mol. Biol.* *20*, 267–273.
- Tam, W.L., Lim, C.Y., Han, J., Zhang, J., Ang, Y.S., Ng, H.H., Yang, H., and Lim, B. (2008). T-cell factor 3 regulates embryonic stem cell pluripotency and self-renewal by the transcriptional control of multiple lineage pathways. *Stem Cells* *26*, 2019–2031.
- Tóth, K.F., Knoch, T.A., Wachsmuth, M., Frank-Stöhr, M., Stöhr, M., Bacher, C.P., Müller, G., and Rippe, K. (2004). Trichostatin A-induced histone acetylation causes decondensation of interphase chromatin. *J. Cell Sci.* *117*, 4277–4287.
- Valouev, A., Johnson, S.M., Boyd, S.D., Smith, C.L., Fire, A.Z., and Sidow, A. (2011). Determinants of nucleosome organization in primary human cells. *Nature* *474*, 516–520.
- Wendt, K.S., and Grosveld, F.G. (2014). Transcription in the context of the 3D nucleus. *Curr. Opin. Genet. Dev.* *25*, 62–67.
- Widom, J. (1992). A relationship between the helical twist of DNA and the ordered positioning of nucleosomes in all eukaryotic cells. *Proc. Natl. Acad. Sci. USA* *89*, 1095–1099.
- Wombacher, R., Heidbreder, M., van de Linde, S., Sheetz, M.P., Heilemann, M., Cornish, V.W., and Sauer, M. (2010). Live-cell super-resolution imaging with trimethoprim conjugates. *Nat. Methods* *7*, 717–719.
- Woodcock, C.L., Skoultchi, A.I., and Fan, Y. (2006). Role of linker histone in chromatin structure and function: H1 stoichiometry and nucleosome repeat length. *Chromosome Res.* *14*, 17–25.
- Wray, J., Kalkan, T., and Smith, A.G. (2010). The ground state of pluripotency. *Biochem. Soc. Trans.* *38*, 1027–1032.
- Yi, F., Pereira, L., and Merrill, B.J. (2008). Tcf3 functions as a steady-state limiter of transcriptional programs of mouse embryonic stem cell self-renewal. *Stem Cells* *26*, 1951–1960.
- Ying, Q.L., Wray, J., Nichols, J., Battle-Morera, L., Doble, B., Woodgett, J., Cohen, P., and Smith, A. (2008). The ground state of embryonic stem cell self-renewal. *Nature* *453*, 519–523.